UNIVERSITY OF CALIFORNIA

SANTA CRUZ

LOWER CRUSTAL XENOLITHS OF THE SOUTHERN SIERRA NEVADA: A MAJOR ELEMENT AND GEOCHRONOLOGICAL INVESTIGATION

A thesis submitted in partial satisfaction of the requirements for the degree of

MASTER OF SCIENCE

In

EARTH SCIENCES

by

Adrienne Grant

December 2016

The Thesis of Adrienne Grant is approved:

_____
Professor Terrence Blackburn, Chair

_____
Professor Jeremy Hourigan

_____
Professor Elise Knittle

_____
Tyrus Miller
Vice Provost and Dean of Graduate Studies

Table of Contents

List of Figures

List of Appendices

Abstract; Lower Crustal Xenoliths of the southern Sierra Nevada: A major element and geochronological investigation, Adrienne Grant

The continental crust is a chemically distinct geochemical reservoir of the bulk silicate Earth that has formed near continuously over the last 4 billion years and is preserved by its intrinsic buoyancy relative to its oceanic counterpart. Rare earth element patterns imply that continental crust is formed at subduction zone settings and yet the primary melts produced by flux melting of the mantle here are basaltic in composition. An additional process is necessary to differentiate these melts to the Si-rich character of continental crust. The models proposed for differentiation includes fractional crystallization and partial melt extraction, which differ greatly in the resulting lower crustal compositions and the timing of formation relative to Si-rich melts. Here we propose that the investigation of the lower crust composition and timing provides one way to distinguish between these two mechanisms. A study was undertaken to characterize lower crustal xenoliths that are inferred to be related to granitoid plutons from the Southern Sierra Nevadas; the Dinkey Creek and Red Lake granodiorites specifically. Thirteen lower to mid-crustal xenoliths were analyzed for major element chemistry and U-Pb geochronology. We suggest that the broad range in chemistry seen in these lower crustal xenoliths can only be derived by the multiple steps and continuous evolution of fractional crystallization. The ages of these xenoliths record magmatism contemporaneous with the upper crustal granitoid plutons. The mafic lower crustal rocks yield zircon U-Pb dates that are younger than their upper felsic counterparts. This is interpreted to reflect a difference in

temperature and crystallization sequence anticipated for mafic and felsic bodies. A summary is developed for the genesis of these plutons and their corresponding mafic cumulate, leading to the generation of crust matching current bulk continental crust estimates.

Introduction

The Earth is unique in the fact that it has a bimodal elevation profile due to two dominant types of crust. There is oceanic and continental crust and they vary most significantly in their chemistry and density. The oceanic crust is basaltic, more dense and ~10 km thick, while the continental crust is andesitic in composition (e.g. ~60% SiO_2), more buoyant and ~40 km thick (Christensen & Mooney, 1995). Their density difference is the dominant control on elevation and it also affects their tectonic properties. When the two types of crust meet at a convergent margin, the buoyancy of the continental crust prevents subduction, and explains the antiquity of continental crust, while the younger oceanic crust gets pushed below and recycled into the mantle (Taylor & McLennan, 1985). The setting of ocean subduction results in arc magmatism, expressed at the surface as volcanic arcs and beneath as sub-arc felsic batholiths. Here, peridotitic mantle undergoes melting as a result of volatile addition, which reduces the melting point of peridotite. Continental crust, like most igneous rocks, is formed by partial melts from the mantle (Rudnick, 1995). On the basis of rare earth element (REE) chemistry, among other things, continental crust is implied to form in subduction zones (Jagoutz and Keleman, 2015). In subduction zones, melts are formed by flux melting from fluids coming off of the subducted slab, as well as decompression melting in the mantle wedge (Grove et al., 2003; Annen et al., 2005). These melts, like in most other settings, are mafic in character. The bulk continental crust itself is not mafic though, and it remains uncertain how it reaches

~60% SiO_2 (Tatsumi and Eggins, 1995, Jagoutz, 2010). The two possible mechanisms proposed for the development of Si-enriched liquids from basalts are partial melting and fractional crystallization. Partial melting involves a secondary heat source being imposed on already solidified basalt/amphibolite, where its excess heat begins to melt the least refractory components of primary subduction zone melts (Annen et al., 2005). Fractional crystallization is a fundamental concept in geology that involves crystallization from a melt where crystals are continuously being removed from the melt, changing its composition (Wilson, B.M., 1989). Following a summary by Jagoutz and others (2009), experimentally generated high pressure partial melting of a natural amphibolite and found that partial melting creates a bimodal chemical pattern with restricted major element compositions for residues and melts (Wolfe and Wyllie, 1994)(Figure 1). Fractional crystallization of hydrous basalts at high pressure creates melt compositions similar to partial melting, but its cumulate compositions differ strongly from partial melting residues, displaying a wider range of compositions in a "zig-zag" shape (Jagoutz et al., 2009) (Figure 2). This occurs as new minerals begin to form within the crystallization sequence, each of which incorporates cations and silica in variable amounts. Another way in which these models differ is their timing. Partial melting models require that a previously emplaced and cold lower crust undergoes partial melting during a later heating event. The age of this earlier crust could potentially be far older than the upper crustal plutons (Annen et al., 2005). As partial melting progresses, the very first melts will be the most felsic and progressively become more mafic (Gill, 1981). With fractional

crystallization, the lower crust and upper crust will be generally contemporaneous with mafic cumulates forming first and the most Si-enriched rocks crystallizing last (Jagoutz et al., 2009).

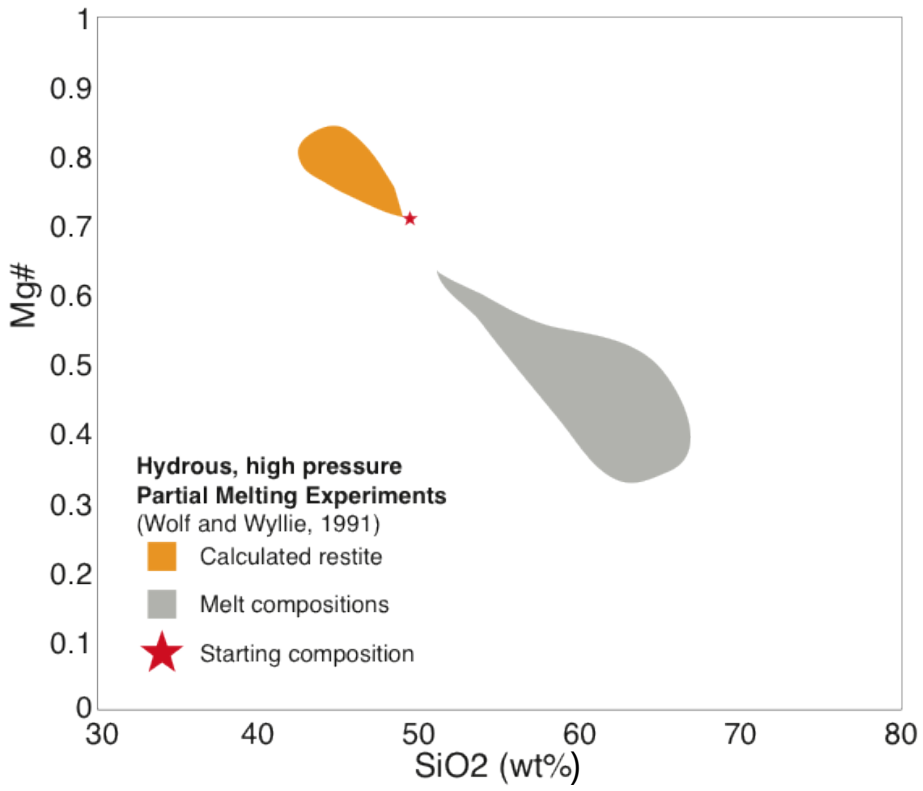

Figure 1. Experimental results for melt compositions generated by partial melting of hydrous basalts at high pressure.

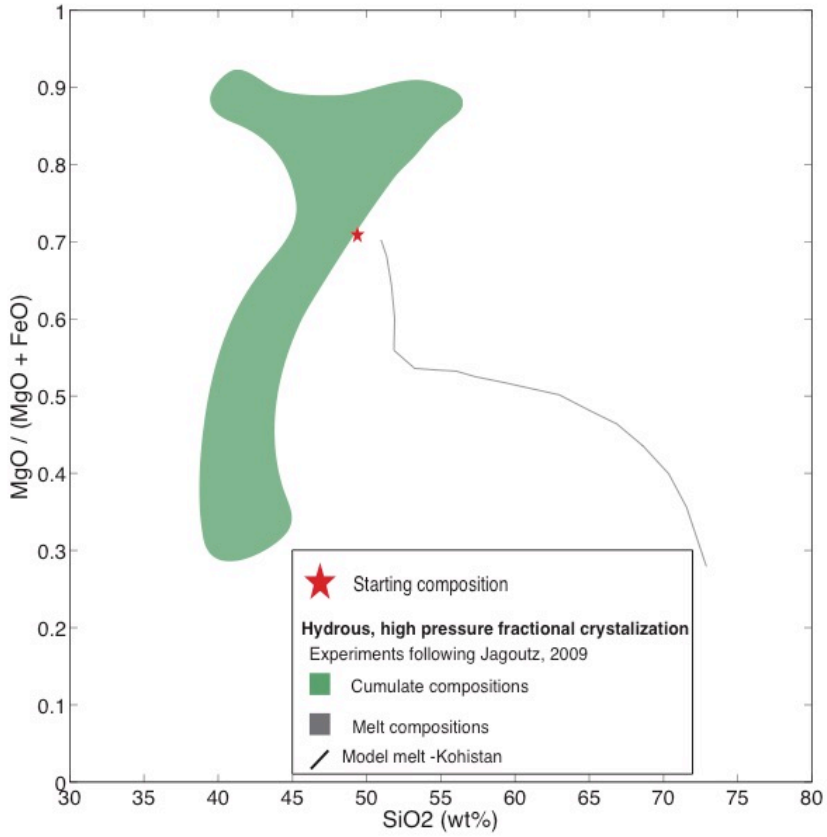

Figure 2. Experimental results for melt compositions generated by fractional crystallization of hydrous basalts at high pressure. Note the large range of values for cumulate compositions

The most obvious differences between processes are seen in the cumulate and restite compositions and their ages, therefore that is what needs to be investigated to determine which process is occurring. These rocks are the complement to the upper crustal plutons and consequently make up the lower crust. This makes the lower crust the key to determining whether partial melting or fractional crystallization is the dominant process. Unfortunately, the inaccessibility of the lower crust make its study and characterization challenging (Rudnick and Fountain, 1995). Exposed granulite terranes were once thought to be representative of the lower crust but a major tectonic

event is required to bring these to the surface and they are chemically more similar to evolved melts (Bohlen et al. 1985, Rudnick & Fountain, 1991). The only other windows to the lower crust are volcanically entrained xenoliths from basalts or kimberlites. These xenoliths are applicable to studies of bulk composition and petrologic processes but they are of limited value for investigating contact relationships or volumetric abundances (Rudnick & Taylor, 1987). A benefit of xenolith-derived zircon is that it has resided at high temperatures and pressures that anneal out most radiation damage, reducing lead loss and discordance (Hanchar & Rudnick, 1995).

To determine the processes that contribute to continental crustal generation we did a number of things. First, a suite of xenoliths of varying compositions representing the lower to middle crust was obtained, as well as samples of their complementary upper crustal plutons. Categorization of their major element properties illuminates the processes by which they were formed and evolved, and if they are complementary to the upper crustal granitoids. Zircon U-Pb dating of this suite of rocks can determine if they are indeed linked in time and will delineate the timescales of lower and upper crustal generation and how they may be related.

Geologic Background

The Sierra Nevada Mountain range lies west of the Basin and Range province, forming one of North America's westernmost mountain ranges, spanning 400 miles north to south. The Sierra Nevadan arc was active from ~200 to 80 Ma, during the

subduction of the Farallon plate under the North American plate. This resulted in the construction of the extensive Sierra Nevada batholith that has been exhumed by faulting and is now exposed at the surface. The batholith shows compositional changes from west to east, with gabbros and diorites to the west and then increasing in silica, becoming predominantly granodiorite in the east (Bateman, 1992). In the latest Cretaceous slab flattening and mantle lithosphere removal began the process of exhumation, with steeper slab dips and slab segmentation in the Central Sierra Nevada causing less uplift (Saleeby et al., 2003). This, as well as the more recent uplift (5-10 Ma), brought up the batholith, exposing rocks as deep as 25-30 km at the southern end, creating an oblique section through the batholith (Saleeby, 1990). This cross section can be extended to depths over 100 km by lower crustal and mantle xenoliths of known depths from the Huntington Lake region (Figure 3).

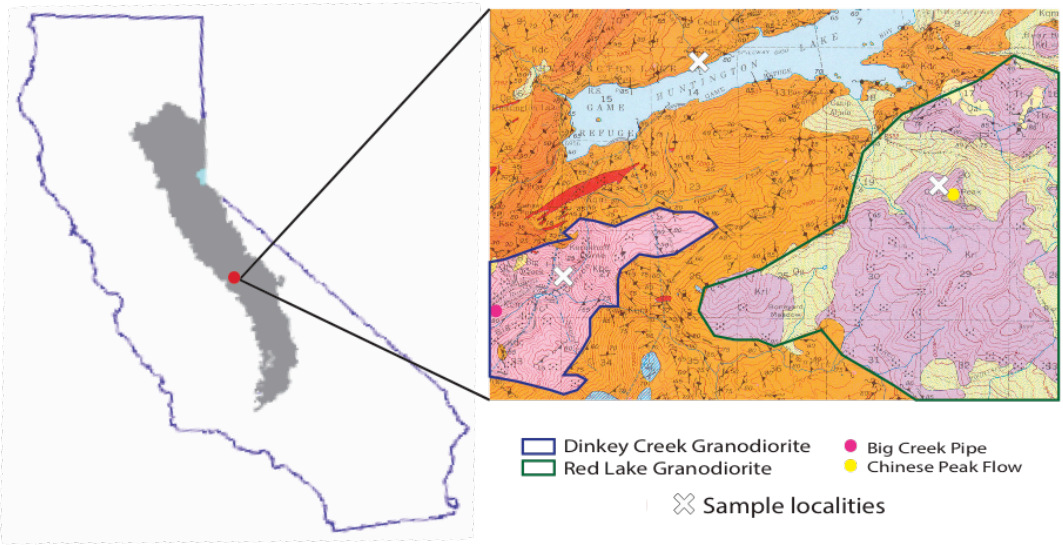

Figure 3. General map of the Sierra Nevada with expanded local map of study area

The main study site is located in the northeast corner of the Huntington Lake quadrangle (Bateman and Wones, 1972). In this area, there are 2 large felsic plutons, Dinkey Creek at 104 Ma and Red Lake at ~90 Ma (Stern et al., 1981). The Dinkey Creek pluton exhibits a strong concentric zonation, with an equigranular rim and megacrystic core, whereas Red Lake is not zoned, purportedly due to early expulsion of volatiles (Noyse, 1983). Studies within these and nearby plutons have aimed to characterize the range of mafic magmatic enclaves (MMEs) observed within their felsic hosts (Barbarin, 2005). A small population of these MMEs demonstrate cumulate texture and have been interpreted to be cumulates that were disrupted and entrained by the granite.

Xenoliths brought up by Miocene volcanism are our window to the lower crust of this region (Dodge et al. 1986, Mukhopadhyay and Manton 1994, Ducea and Saleeby 1998a). Dodge (1986) describes these xenoliths at 2 sub-sites, one in Big Creek and the other at the top of Chinese Peak in ~10 Ma basalt flows (Figure 3). The Big Creek xenoliths suites are dominated by eclogite and garnet granulites, with less abundant peridotites and feldspathic granulites, and rare pyroxenites (Dodge et al., 1986). The China Peak xenoliths are dominantly pyroxenites and feldspathic granulites, with rare peridotites (Dodge et al., 1986). There is a distinct lack of garnet within the China Peak xenolith suite and this has been inferred to indicate that these rocks experienced pressures of no more than 10 kb (Green and Ringwood, 1967; Ito and Kennedy, 1971). All of these rocks are silica-undersaturated, indicating that the lower crust in this region is mafic-ultramafic (Dodge and Bateman, 1988).

Methods

Samples were newly collected in Big Creek and from the China Peak mountain resort, while previously collected samples were borrowed from the Frank Dodge collection at the Smithsonian. Fist sized separates were crushed in a shatterbox and separated both magnetically and with heavy liquids. Zircon crystals were picked from these grain separates, mounted in epoxy and polished to expose their cores for imaging. Imaging was done on the scanning electron microscope (SEM) at Stanford University. Cathodoluminescence (CL) imaging illuminates chemical variation in the crystal that is not visible otherwise and can screen for metamorphic or igneous zoning patterns (Hanchar & Rudnick, 1995) that enable selection of acceptable spots for laser ablation. Laser ablation inductively coupled plasma mass spectrometry (LA-ICPMS) analyses were done on selected grains, using the U/Pb system, to determine rough ages and to interpret core and rim ages within crystals. Rock chips from new samples and selected Smithsonian samples were also sent for X-ray Fractionation (XRF) whole rock major element geochemistry to ALS Global, where they were crushed, fused and analyzed. Previous geochemical analyses from the literature (collected from EarthChem; Dodge et al. 1986, Ducea and Saleeby 1998a, Mukhopadhyay and Manton 1994, Sisson et al 1996, Ducea 2002, Lee et al, 2006) are also utilized in the interpretation presented here.

Results

Igneous textures were widely seen in the zircon CL images and these zones were used to establish the analysis spots so igneous crystallization ages were yielded. Two populations can be determined for 15-CP-01 by CL zones. One has thick detailed igneous growth zones in which many layers are bright and some show resorptive edges. The other population is darker and less detailed, with CL dead rims and/or mantles and cores (Figure 4). Granodiorite sample 15-CP-03 has more abundant resorptive boundaries between growth zones and some very dark CL cores (Figure 6, inset CP-03). Sample 15-CPX-02 showed dominantly indistinct dark zones in CL, with minor vaguely igneous cores and dominant bright metamorphic rims (Figure 6, inset CPX-02). The tonalite 15-CPX-03 showed dominantly igneous zoning with some CL dead cores and some evidence of multiple igneous events. Another tonalite, 15-CPX-04, is similar to 15-CPX-03 except there are much thicker and more predominant metamorphic rims (Figure 5). The diorite 15-CPX-05 zircon grains predominantly displayed cores with igneous growth zones and thicker, very bright metamorphic rims (Figure 6, inset CPX-05). The pyroxenite sample 15-CPX-06 was dominantly bright and igneous but showed evidence of metamorphism and resorption between igneous events (Figure 6, inset CPX-06 shows complex zones). Amphibolite 116478-0023 displayed pervasive metamorphic rims with dark to bright igneous cores as well as metamorphically altered cores (Figure 6, inset 0023). Garnet granulite 116478-0027 was composed of mostly CL bright, indistinctly zoned grains with minor darker igneous cores (Figure 6, inset 0027). Gabbro 116478-0238

displayed rare igneous cores with metamorphic rims and was mostly composed of complex or indistinct zoning. Granulite 116478-0296 was predominantly indistinct dark grey in CL with minor bright metamorphic rims and CL dead cores (Figure 6, inset 0296).

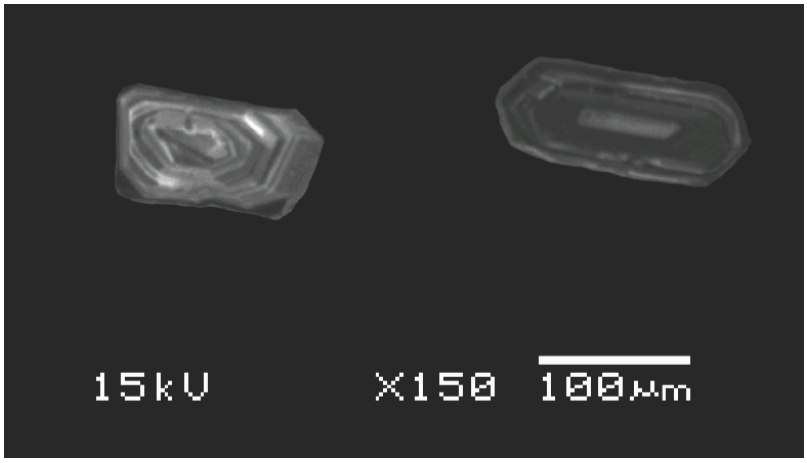

Figure 4. Cl populations of 15-CP-01. Detailed igneous zones on the left and dull, darker zones on the right

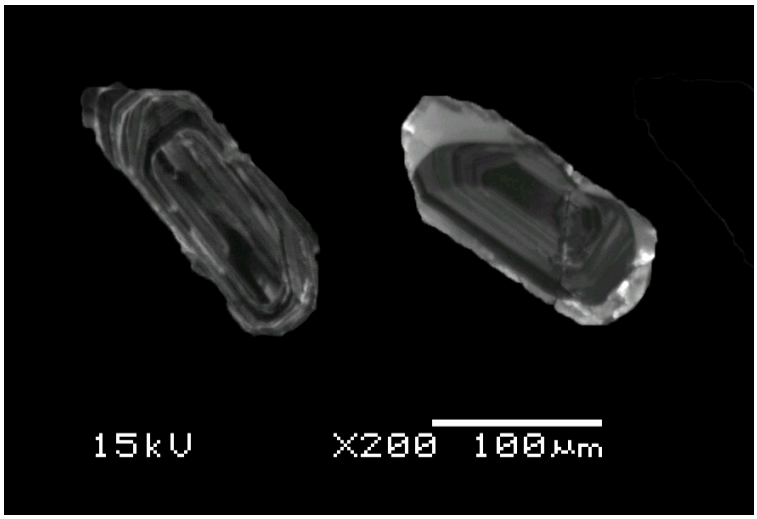

Figure 5. Representative CL photomicrographs of tonalite samples 15-CPX-03 and 15-CPX-04, left and right respectively.

Here we report the error-weighted mean ^{238}U-^{206}Pb zircon dates were calculated from laser ablation data. The amphibolite from Big Creek, 116478-0023, has a zircon age of 100.57±0.93 Ma. Also from Big Creek, 116478-0027, a garnet granulite was dated at 96.5±1.2 Ma. 116478-0238, a gabbro from Big Creek, has zircons that are 95.3±1.3 Ma. 116478- 0296, a granulite from China Peak, has a zircon age of 96.4±1.3 Ma. The Dinkey Creek granodiorite adjacent to an aplite dike was dated at 100.60±0.78 Ma. The equigranular phase of the Dinkey Creek granodiorite 15-CP-03 has a mean zircon age of 102.31±0.49 Ma. Sample 15-CPX-02 is hard to determine a lithology for, as it looks like it was once a fine-grained pyroxenite but has been overprinted with quartz veins and metasomatised. It has a zircon crystallization age of 95.8±2.1 Ma. Sample 15-CPX-03 is a tonalite from China Peak. This sample has a bimodal size distribution of zircon but their ages are indistinguishable, both coming in at around 102 Ma. 15-CPX-04 is another tonalite from China Peak that yields a bimodal age distribution that correlates with zircon size. The large zircon grains are 94.4±1.2 Ma and the small are 100.1±1.1 Ma. A diorite from China peak, sample 15-CPX-05, has a zircon age of 96±1.8 Ma. At 89.1±1.8 Ma, sample 15-CPX-06 is a pyroxenite and the youngest dated sample. The rocks analyzed comprise an age range of ~89 – 102 Ma (Figure 4). Most age populations analyzed show an expansive age range and no statistically significant weighted mean population with mean standard widths of deviation (MSWDs) of 1.6 to 24. The overall trend observed indicates that the more mafic xenoliths are the youngest while the granites and felsic xenoliths are the oldest.

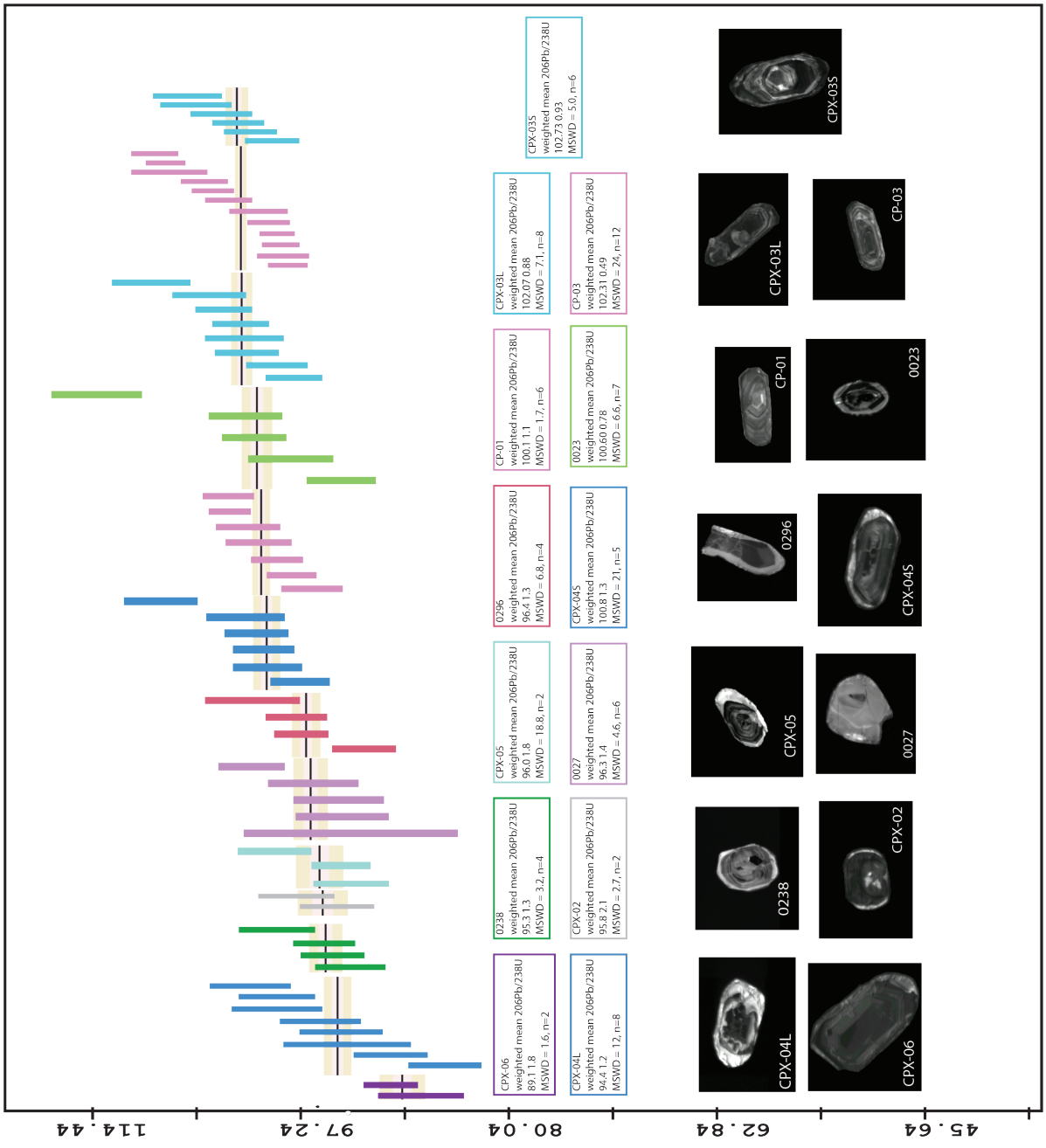

Figure 6. Compiled weighted mean plot of zircon dates from selected samples

The samples analyzed span a range of compositions from clinopyroxenite to monzogranite and the XRF data can further determine rock types. The Mg # (Mg/Mg+FeT) is used as a differentiation index. These Mg# values show a large spread vs SiO_2 with each lithology slightly clustered. Age vs compositional differentiation indices was also plotted to illuminate age progression and differentiation. The samples came from both Big Creek and China Peak, which have different aged plutons, and no pattern was immediately recognizable.

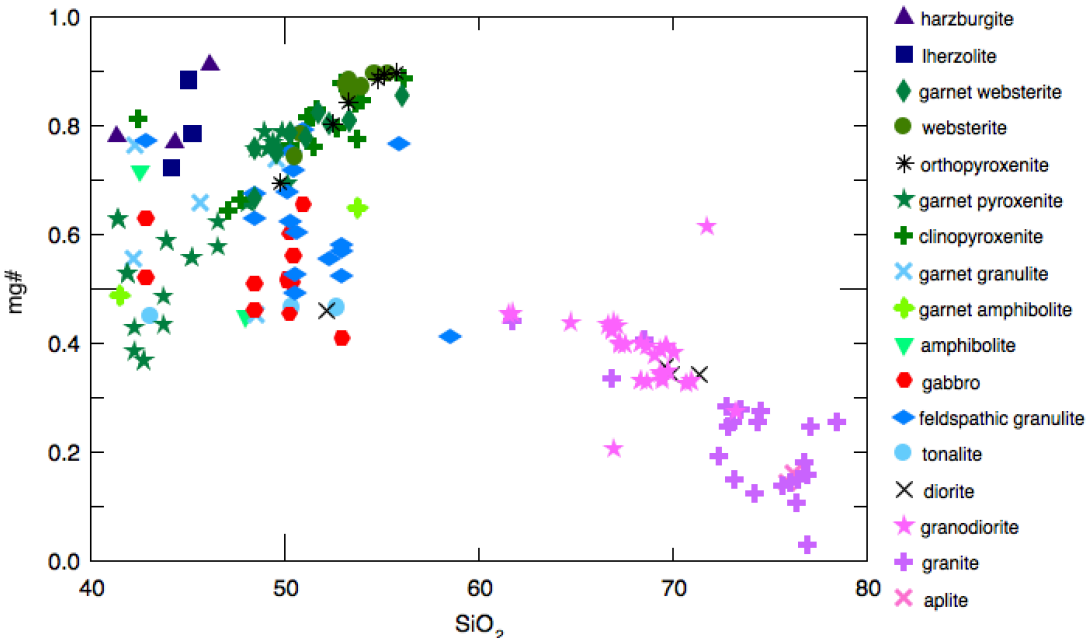

Figure 7. Mg# versus wt% SiO2. Combined literature data and new results (Dodge et al. 1986, Ducea and Saleeby 1998a, Mukhopadhyay and Manton 1994, Sisson et al 1996, Ducea 2002, Lee et al, 2006).

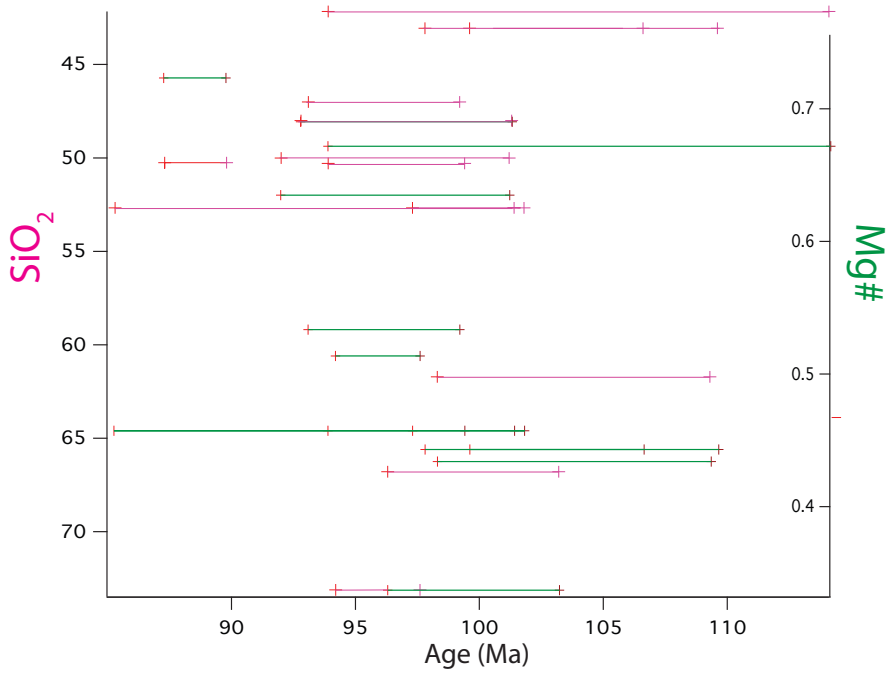

Figure 8. Minimum and maximum sample age versus wt% SiO_2 (pink) and Mg# (green). New data only.

Discussion

Cathodoluminescence imaging reveals structures that are otherwise invisible in normal optical microscopy such as compositional zoning of the elements Zr, Si, Hf, P, Y, REEs, U and Th (Hanchar and Rudnick 1995, Corfu et al., 2003). The types of zoning seen in CL can indicate the crystallization environment, with metamorphic and igneous growth zones looking distinctly different, while the overall morphology can distinguish crystallization speed (Mattinson et al. 1996, Corfu et al., 2003). Diffusion of the trace elements in the zircon crystal structure that control CL is incredibly slow, allowing for multiple crystallization events occurring over

geologically long time periods to be preserved in a single crystal (Cherniak et al., 1997a).

The deeper xenolith samples were significantly more CL active than the granites or shallower xenoliths. Per Hanchar and Rudnick (1995), this is likely due to longer times at depth and/or pressure that would anneal damage and allow CL to be more distinct. Pervasive CL-bright rims and overgrowths (Figure 7) are interpreted to indicate a metamorphic event at some point after initial crystallization age. The occurrence of metamorphic cores and alteration is not surprising, as the western margin of North America was tectonically active in the late Mesozoic and early Cenozoic. The zircon CL images that demonstrate multiple igneous events often have resorptive boundaries between them. This may indicate magma chamber processes, such as re-equilbration with the melt, but may also be indicative of inherited cores sourced from the melt or wallrock. Inherited cores have been noted in Sierra Nevada plutons by multiple studies (Coleman et al. 2004, Saleeby et al. 1987) and geochronologic analyses of different CL zones can substantiate this. Overall, the zoning seen is a good indicator that we are definitely looking at igneous, and not metamorphic, rocks. Many of the historically collected xenolith samples were designated metamorphic rock names. A further look into trace elements could give proof of igneous origin, but the CL and thin section textures are a good start. There is some evidence of metamorphism in the thin sections (minor Ostwald ripening, reaction textures related to metasomatism) but overall the textures are indicative of igneous origin.

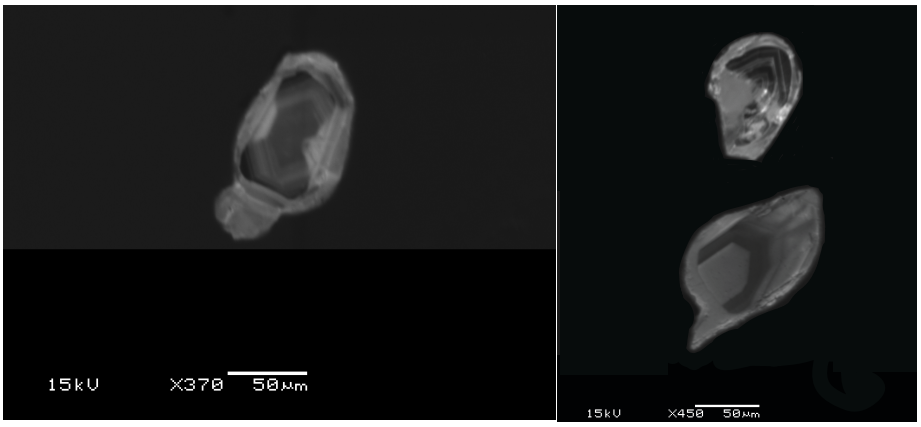

Figure 9. CL images showing zircons with metamorphic rims and overgrowths

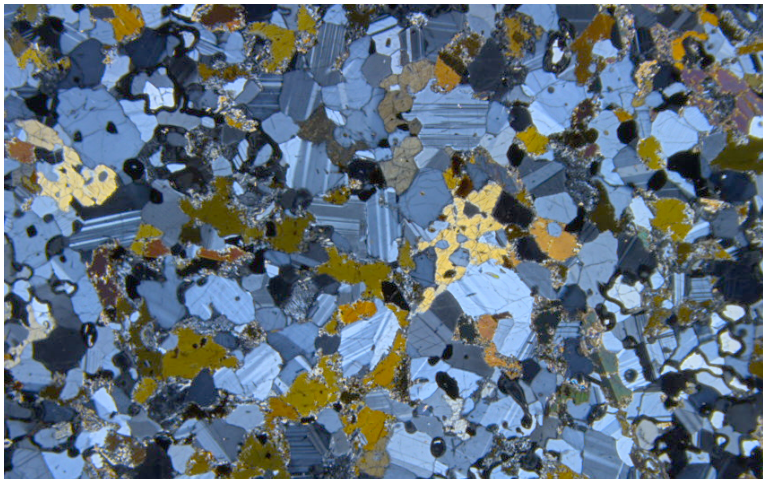

Figure 10. Cumulate textures in sample 116478-0027, a "hornfels" collected by Dodge (1986)

Big Creek xenoliths tend to be younger than their pluton, while China Peak xenoliths tend to be older with both xenolith suites occupying the same age range between ~90 and ~104 Ma. The tonalite samples that showed bimodal size populations, 15-CPX-03 and 15-CPX-04, produced very similar ages for both. The small zircons were likely trapped as mineral inclusions, inhibiting their size, or the large ones just grew quicker within the resolvable scale. There is a slight trend of

mafic rocks being the youngest with the most felsic rocks crystallizing later. This may be due to sampling bias, as our granites are from the older pluton and our most mafic xenolith is from the younger. It is also possible that this is simply due to crystallization depth. As the mafic cumulates reside at depth, while the Si-enriched melts ascend, ambient temperatures around each lithology will be different. This will likely affect cooling rates, potentially slowing the mafic crystallization rates enough to allow the felsic rocks to crystallize first. As well, zircon crystallization properties will have zircon crystallizing at a later stage in the mafic rocks, whereas zircon is an early crystallizing phase in felsic rocks.

This is strong evidence in support of fractional crystallization. It seems that the progressive lithological phases are cogenetic, at least in time. With no significant jumps in time along the series of progressive Si-enrichment, the age pattern is consistent with fractional crystallization models (Winter, 2001). With repetitive basaltic sills underplating the crust, magmatic activity was likely constant, with lulls in between large pluton building pulses (Annen et al., 2005; Coleman et al., 2004). There is a strong presence of ~95 Ma dates that doesn't attribute to any exposed pluton. This observation implies that there could be a ~95 Ma pluton that stalled lower than the current surface or that this melt didn't evolve to as high Si content. Melts coming from progressive sills should be of similar chemistry but there's enough variation in water content in typical basalts that regular variability could have produced a deeper stalling melt (Barclay & Carmichael, 2004; Coleman et al., 2004,).

The fact that many of the xenoliths are younger than their plutons is not entirely surprising; Rudnick and Gao (2003) noted that this was common. It must also be considered that these ages are zircon crystallization ages and different minerals crystallize out at different stages of solidification. Zirconium must saturate in the melt for zircon to crystallize. In addition, zircon formation displays a dependence on the composition of the magma, where for any given Zr concentration, a mafic melt will form zircon at lower temperatures compared with a more felsic composition (Hanchar & Watson, 2003). The bulk composition zircon saturation temperatures predicted for many Sierran xenoliths are below 600 C, temperatures at which the rock is entirely solid. And yet zircons are present within these mafic restite/cumulates. This likely reflects the concentration of zirconium within a slowly cooling melt—an observation that seems to point to fractional crystallization as the process by which mafic lower crust is generated. Additionally, the geotherm has been seen to have a large influence on crystallization and differentiation (Annen et al. 2005). Melt viscosity depends strongly on dissolved H_2O and temperature, and when melts reach H_2O saturation, the water exsolves from the melt and crystallization progresses much faster. The loss of water increases viscosity, prohibiting further ascent. Annen and others (2005) address this in detail and interpret it as the overriding factor for controlling where each composition resides in the crust. The geotherm also influences whether lower crustal partial melting will contribute. If the crust is thick enough that the amphibolite liquidus is crossed, the lower crust, if fertile, can contribute partial melts (Jagoutz, 2010). Many models of continental crust

formation also require a modicum of assimilation to acquire certain chemical traits (DePaolo, 1981, Annen et al., 2005). Sisson et al. (2005) took samples from sheeted mafic sills in the Sierra Nevada region, typifying mafic liquids present during batholith growth, and experimentally recreated high pressure crystallization from these melts without specifying whether these melts were primary or partial melts of existing rocks. High K granites, similar to average upper continental crust, were created proving that continental crust can be derived solely from these sources. Ratajeski et al. (2005) experimentally derived felsic melts from partial melting of hydrous gabbroic rocks from the Onion Valley complex. These experimentally derived melts matched felsic plutons in the Sierra Nevada. In this experiment though, only the evolved melts were studied and not the remaining cumulates or restites. As shown in figures 2 and 3, partial melting and fractional crystallization both generate fairly similar felsic melts but substantially different cumulate and restite compositions. This study creates an attractive premise but must be looked at deeper.

Figure 8 shows Mg# vs SiO_2 for xenoliths and granitoids in our study region and the xenoliths occupy a large range of Mg# similar to that modeled for fractional crystallization. This large range of chemistries is caused by repeated crystallization events where the melt is continuously being segregated from its crystal mush. This segregation inhibits equilibrium crystallization as the melts and the solids are no longer in contact. Therefore the melt chemistry evolves as certain minerals take different elements out of the system, starting with Mg and Fe and other compatible

elements. The data points show an expansive spread that could only be produced by multiple steps of crystallization and melt evolution/segregation.

One problems with the fractional crystallization model is the necessary highly volumetric complementary mafic cumulate to the upper crustal granitoids (Annen et al, 2005). Bulk crust compositions require this to be removed and seismographic imaging shows that this is not present below the Sierra Nevada batholith in this region (Zandt et al., 2004). A method of removal or delamination is thus needed to account for its absence. If the source of the basalt is underplating sills at the base of the crust (Annen et al., 2005), this becomes more congruent with the proposed model, as the most mafic cumulates can very easily eclogitize or use their inherent density disparity to delaminate and sink into the mantle. Müntener and Ulmer (2006) interpreted that ~12% trapped liquids is sufficient to stabilize dense ultramafic cumulates and delamination will not occur until after a substantial period of cooling. This is congruent with extensive Pliocene uplift in the region ~70 Ma after intrusion. Wernicke et al. (1996), interpreted their seismic experiments as proof of an absent large crustal root. The observed high elevations thus necessitate and underlying buoyant low-density mantle. Boyd et al., (2004) have used teleseismic events to tomographically model the crust below the Sierras and they appear to have imaged an eastward-tilting block of approximately 30% garnet and 70% pyroxene that is in the process of delaminating from the crust. This is supported by changing chemistry in the xenoliths brought up by Neogene basalts, as sometime after 10 Ma, the xenoliths begin to demonstrate fertile mantle compositions (Lee et al., 2001). Disparities in the

crust-mantle Mohorovic discontinuity also infer a downwelling "drip" of dense lower crust that has foundered away (Zandt et al., 2004). Zones where the Moho is obscured or broad have also been linked to fractional crystallization of ultramafic cumulates at depth (Müntener & Ulmer, 2006).

As the subduction of the Farallon plate progressed, dehydration reactions off the descending slab fluxed the overlying mantle and some decompression melting in the mantle wedge generated basaltic melts that formed sills or ponded at the base of the crust. These basaltic melts partially crystallized, leaving behind an ultramafic cumulate while the remaining melt began to ascend due to density and viscosity contrasts. Due to a variety of factors, these melts stalled in the upper crust where they crystallized and formed the extensive Sierra Nevada batholith. Later volcanism brought up pieces of this lower crust as xenoliths. Subduction proceeded until there were no more melts being created. Much later in time, ~70 My, as the newly generated lithosphere cools and all the melt has solidified, the density contrast increases to a critical point and the lower crustal mafic cumulates begin to founder back into the mantle. This process and its counter-flow replaced the dense cumulates with more buoyant asthenosphere, and along with extension in the Western US operating between ~25-10 Ma, created uplift and exhumed these plutons to where we see them today. This basalt evolution generating felsic melts, paired with the loss of the mafic cumulate, allows the crust to reach an expected bulk andesite composition.

Conclusion

Major element patterns in the Sierra Nevada xenoliths strongly support a fractional crystallization origin. A near continuous suite of compositions between mafic and felsic end members is also of note. Age relationships do not irrefutably discount partial melting, but their progression in time to more Si-enriched rocks is not inconsistent with fractional crystallization models. This provides a solid baseline for application of this model as the modern generator of continental crust. Consequently, we have a foundation for greater understanding of crustal evolution through time and how the current heterogeneous felsic continental crust was generated. A more thorough examination of the sample dates with a higher precision method may give deeper insight into magmatic timescales within the cumulates and trace element analysis could be used to further delineate the petrogenetic processes at work.

Appendix 1. Major Element XRF data for analyzed samples

Rock Type	Sample Name	Al2O3	BaO	CaO	Cr2O3	Fe2O3	K2O	MgO	MnO	Na2O	P2O5	SO3	SiO2	SrO	TiO2
granite	15-CP-01	17.42	0.04	3.19	0.01	3.9	1.46	1	0.12	4.99	0.08	0.11	66.79	0.03	0.43
granite	15-CP-02	12.91	0.03	1.3	0.02	1.43	2.73	0.24	0.03	4.11	0.03	0.04	77.02	0.01	0.14
granite	15-CP-03	16.08	0.08	5.2	0.01	6.4	2.37	2.56	0.11	3.15	0.17	0.02	61.71	0.04	0.78
granite	15-CP-04	15.16	0.13	2.83	0.01	3.25	3.3	1.13	0.06	3.56	0.13	<0.01	68.46	0.06	0.45
too altered	15-CPX-01	3.14	0.03	3.3	0.59	8.23	1.03	27.5	0.15	0.79	0.01	<0.01	55.16	0.01	0.14
too altered	15-CPX-02	8.67	0.02	7.88	0.02	4.79	0.09	2.71	0.06	0.4	0.2	<0.01	73.11	0.03	0.43
tonalite	15-CPX-03	17.78	0.05	10.5	<0.01	17.3	0.13	7.2	0.22	0.83	0.31	0.21	43.06	0.07	2.39
tonalite	15-CPX-04	20.46	0.04	7.97	0.01	8.65	0.31	3.83	0.12	4.19	0.24	<0.01	52.67	0.11	1.08
anorthosite	15-CPX-05	21.46	0.04	6.83	<0.01	9.33	0.71	2.85	0.14	3.73	0.38	<0.01	50.29	0.11	1.45
pyroxenite	15-CPX-06	5.49	0.01	15.9	0.49	9.76	0.09	15.25	0.14	1.13	0.02	0.15	50.25	0.02	0.33
pyroxenite	15-CPX-07	5.25	0.01	10.25	0.29	9.66	0.06	21.9	0.16	0.45	0.01	0.02	51.38	0.01	0.25
pyroxenite	15-CPX-08	4.41	0.02	14.4	0.24	8.71	0.4	17.2	0.18	0.9	0.04	0.01	52.65	0.02	0.34
gabbro	15-CPX-09	18.37	0.03	9.3	0.01	9.74	0.81	5.21	0.14	3.02	0.46	<0.01	50.32	0.08	1.26
garnet amphibolite	116478-16	17.64	0.08	11.85	0.01	5.08	0.93	4.79	0.09	3.68	0.61	0.01	53.69	0.11	0.2
garnet amphibolite	116478-44	17.26	0.03	12.05	0.02	15.5	0.44	7.51	0.18	1.7	0.49	0.14	41.45	0.05	2.25
amphibolite	116478-57	19.53	0.05	8.72	<0.01	11.74	1.04	4.88	0.14	3.88	0.4	0.03	47.94	0.1	1.4
garnetite	116478-122	17.49	0.03	11.25	0.02	16.96	0.33	10.75	0.36	0.73	0.05	0.49	42.16	0.01	0.48
amphibolite	116478-153	20.9	0.02	12.3	0.02	8.58	0.55	11.05	0.13	1.56	0.03	0.01	42.5	0.08	0.39
granulite	116478-289	18.36	0.05	8.64	0.02	12.18	0.85	5.11	0.16	2.83	0.43	0.01	48.46	0.09	1.58

Appendix 2. Brief thin section description of selected samples

Sample name	Rock type	plag	kspar	qtz	bt	hbl	cpx	opx	ox	grt	grain size	texture
15-CP-01	monzogranite	20	50	25	5						coarse	allotriomorphic seriate
15-CP-02	monzogranite		50	40	10						medium	allotriomorphic seriate
15-CP-03	kspar granite	20	30	20	10	20					medium	allotriomorphic seriate
15-CP-04	monzogranite	30	30	30	10						medium-fine	hypidiomorphic seriate
15-CPX-01											fine	acicular
15-CPX-02				30			10	5	30		fine	allotriomorphic seriate
15-CPX-03	tonalite	35		25			5	25	10		fine	allotriomorphic seriate
15-CPX-04	tonalite	60		20				20			coarse	allotriomorphic seriate
15-CPX-05	diorite	60		10	10		10		10		fine-medium	hypidiomorphic seriate
15-CPX-06	websterite						45	35	20		medium-coarse	allotriomorphic seriate
15-CPX-07	webserite						40	40	20		medium	hypidiomorphic equigranular
15-CPX-08	websterite						60	30	10		coarse	allotriomorphic seriate
15-CPX-09	qtz gabbro	30		20	10	20	15	5			fine-medium	allotriomorphic seriate
116478-11	gabbronorite	70				20		5	5		fine	allotriomorphic seriate
116478-16	gabbro	40				10	40			5	medium-coarse	hypidiomorphic bimodal
116478-27	gabbronorite	65					20	10	5		fine to coarse	hypidiomorphic seriate
116478-44	garnet websterite					10	30		10	50	coarse	allotriomorphic seriate
116478-57	hbl gabbro	80				15			5		medium	hypidiomorphic seriate
116478-111	grt hbl clinopyroxenite					45	20			35	medium	hypidiomorphic bimodal
116478-122	grt orthopyroxenite							20		80	medium	hypidiomorphic seriate
116478-153	hornblendite	20				60				20	fine to coarse	hypidiomorphic seriate
116478-289	gabbro	60				5	5		30		medium	allotriomorphic seriate
116478-296	gabbronorite	60					5	10	25		fine-medium	allotriomorphic seriate

Appendix 3. ^{206}Pb-^{238}U Age summary tables for samples interpreted

116478-0023

filename	206/238 age	2SE
11623_9.FIN2	101.8	2.9
11623_10.FIN2	114.1	3.6
11623_11.FIN2	98.1	3.4
11623_17.FIN2	101.1	2.5
11623_20.FIN2	93.9	2.7

116478-0027

filename	206/238 age	2SE
11627_1.FIN2	96.2	3.6
11627_4.FIN2	94.1	3.6
11627_7.FIN2	93.1	3
0027_3.FIN2	101.3	2.6
0027_8.FIN2	93.8	3.7
0027_16.FIN2	93.1	8.7

116478-0238

filename	206/238 age	2SE
116238_2.FIN2	94.6	2.5
116238_3.FIN2	99.2	3
0238_5.FIN2	95.3	2.4
0238_8.FIN2	93.1	2.7

116478-0296

filename	206/238 age	2SE
116296_2.FIN2	92	2.5
116296_6.FIN2	97.2	2.1
116296_9.FIN2	97.6	2.4
0296_16.FIN2	101.2	3.8
0296_17.FIN2	107.5	5.1

15-CP-01

filename	206/238 age	2SE
CP-01_32.FIN2	96.3	2.4
CP-01_10.FIN2	98	1.9
CP-01_28.FIN2	99.2	2
CP-01_13.FIN2	100.8	2.5
CP-01_25.FIN2	101.6	2.5
CP-01_9.FIN2	103.1	1.6
CP-01_19.FIN2	103.2	2

15-CP-03

filename	206/238 age	2SE
CP-03_10.FIN2	98.7	2
CP-03_9.FIN2	99.2	1.3
CP-03_5.FIN2	103.2	1.8
CP-03_12.FIN2	108.4	1.5

15-CPX-02

filename	206/238 age	2SE
CPX-02_11.FIN2	94.2	2.9
CPX-02_13.FIN2	97.6	3
CPX-02_14.FIN2	105.5	2.8

15-CPX-03L

filename	206/238 age	2SE
CPX-03L_42.FIN2	97.8	2.2
CPX-03L_29.FIN2	99.2	2.4
CPX-03L_41.FIN2	101.7	2.5
CPX-03L_39.FIN2	101.9	3.1
CPX-03L_31.FIN2	102.2	2.2
CPX-03L_15.FIN2	103.6	2.2
CPX-03L_35.FIN2	104.8	2.9
CPX-03L_6.FIN2	109.6	3.1

15-CPX-03S

filename	206/238 age	2SE
CPX-03_4.FIN2	99.6	2.1
CPX-03_3.FIN2	101.4	2
CPX-03_2.FIN2	102.4	2
CPX-03_5.FIN2	103.8	2.4
CPX-03_8.FIN2	105.9	2.8
CPX-03_13.FIN2	106.6	2.7

15-CPX-04L

filename	206/238 age	2SE
CPX-04L_17.FIN2	85.3	2.9
CPX-04L_23.FIN2	89.8	2.9
CPX-04L_32.FIN2	93.4	5.1
CPX-04L_12.FIN2	93.9	3.3
CPX-04L_22.FIN2	95.6	3.2
CPX-04L_2.FIN2	99.2	3.6
CPX-04L_10.FIN2	99.2	3
CPX-04L_18.FIN2	101.4	3.2

15-CPX-04S

filename	206/238 age	2SE
CPX-04_7.FIN2	97.3	2.3
CPX-04_13.FIN2	100	2.7
CPX-04_19.FIN2	100.3	2.4
CPX-04_14.FIN2	100.9	2.5
CPX-04_9.FIN2	101.8	3.1
CPX-04_5.FIN2	108.8	2.9

15-CPX-05

filename	206/238 age	2SE
CPX-05_2.FIN2	99.4	2.9
CPX-05_6.FIN2	93.9	2.3

15-CPX-06

filename	206/238 age	2SE
CPX-06_5.FIN2	87.3	3.4
CPX-06_1.FIN2	89.8	2.1

References

Annen, C., Blundy, J.D., Sparks, R.S.J., 2006, The Genesis of Intermediate and Silicic Magmas in Deep Crustal Hot Zones, J. Petrology, 47 (3) 505-539

Barbarin, B., 2005, Mafic magmatic enclaves and mafic rocks associated with some granitoids of the central Sierra Nevada batholith, California: nature, origin, and relations with the hosts, Lithos, 80, 155-177

Barbey, P., Alle, P., Brouand, M., Albarede, F., 1995, Rare-earth patterns in zircons from the Manaslu granite and Tibetan slab migmatites (Himalaya) : insights in the origin and evolution of a crustally-derived granite magma, Chemical geology, 125, 1-17

Barclay J., Carmichael, I.S.E., 2004, A hornblende basalt from Western Mexico: water-saturated phase relations constrain a pressure-temperature window of eruptability, Journal of Petrology, 45, 485-506

Bateman, P.C., and Wones, D.R., 192, Geologic map of the Huntington Lake quadrangle, central Sierra Nevada, California: U.S. Geological Survey Geologic Quadrangle Map GQ-987, scale 1:62,500

Bateman, P.C., Chappell, B.W., 1979, Crystallization, fractionation, and solidification of the Tuolumne Intrusive Series, Yosemite National Park, California, GSA Bulletin, 90, 465-482

Bateman, P.C., 1992, Plutonism in the central part of the Sierra Nevada batholith, California: U.S. Geological Survey Professional Paper, v. 1483, 186 p

Belousova, E.A., Griffin, W.I., O'Reilly, S.Y., Fisher, N.I., 2002, Igneous zircon: trace element composition as an indicator of source rock type, Contrib. Mineral. Petrol., 143, 602-622

Bohlen S.R., Valley, J.W., Essene, E.J., 1985, Metamorphism in the Adirondacks. I. Petrology, Pressure and Temperature, Journal of Petrology, 26, 971-992

Boyd, O. S., Jones, C. H., Sheehan, A. F., 2004, Foundering lithosphere imaged beneath the southern Sierra Nevada, California, USA. Science 305, 660–662

Cherniak, D.J., Hanchar, J.M., Watson, E.B., 1997a, Rare-earth diffusion in zircon, Chemical Geology, 134, 289-301

Christensen, N.I., and Mooney, W.D., 1995, Seismic velocity structure and composition of the continental crust: A global view, J. Geophys. Res., 100(B6), 9761–9788

Coleman, D.S., Gray, W., Glazner, A.F., 2004, Rethinking the emplacement and evolution of zoned plutons: Geochronologic evidence for incremental assembly of the Tuolumne Intrusive Suite, California, Geology, 32, 433-436

Corfu, F., Hanchar, J.M., Hoskin, P.W.O., Kinny, P., 2003, Atlas of Zircon Textures, in Hanchar, J.M., Hoskin, P.W.O., eds., Zircon, Reviews in Mineralogy and Geochemistry, v. 53 p. 469-500, Mineralogical Society of America and Geochemical Society

Davis, D., Williams, I.S., Krogh, T.E., 2003, Historical development of zircon geochronology, Reviews in Mineralogy and Geochemistry, 53, 145-181.

DePaolo DJ, 1981, Trace element and isotopic effects of combined wallrock assimilation and fractional crystallization. Earth Planet Sci Lett, 53,189–202

Dodge, F.C.W., Calk, L.C., Kistler, R.W., 1986, Lower crustal xenoliths, Chinese Peak lava flow, Central Sierra Nevada, J. Petrol., 27, 1277–1304

Dodge, F.C.W., Bateman, P.C., 1988, Nature and origin of the root of the Sierra Nevada, American Journal of Science, 288, 341-357

Ducea, M. N., and Saleeby, J.B., 1998a, The age and origin of a thick mafic-ultramafic keel from beneath the Sierra Nevada Batholith, Contrib. Mineral. Petrol., 133, 169–185

Ducea,M. N. & Saleeby, J. B., 1998b, A case for delamination of the deep batholithic crust beneath the Sierra Nevada, California. Int. Geol. Rev. 40, 78–93

Ducea, M.N., 2002, Constraints on the bulk composition and root foundering rates of continental arcs: A California arc perspective: Journal of Geophysical Research, v. 107

Farmer, G.L., Perry, F.V., Semken, S., Crowe, B., Curtis, D., DePaolo, D.J., 1989, Isotopic evidence on the structure and origin of subcontinental lithospheric mantle in Southern Nevada. J. Geophys. Res., 94: 7885-7898

Gill, J.B., 1981, Orogenic Andesites and Plate Tectonics, Springer-Verlag, 390 pp

Godderis, Y., Donnadieu, Y., Tombozafy, M., Dessert, C, 2008, Shield effect on continental weathering: implication for climatic evolution of the Earth at the geologic timescale, Geoderma, 145, 439–448

Green, D.H., Ringwood, A.E., 1967, Melting and phase relations in an anhydrous basalt to 40 kilobars, Amer. J. Sci., 265, 475-518

Grove, T.L., Elkins-Tanton, L.T., Parman, S.W., Chatterjee, N., Müntener, O., Gaetani, G.A., 2003, Fractional crystallization and mantle-melting controls on calc-alkaline differentiation trends: Contributions to Mineralogy and Petrology, 145, 515–533

Hanchar, J.M., & Rudnick, R.L., 1995, Revealing hidden structures: The application of cathodoluminescence and back-scattered electron imaging to dating zircons from lower crustal xenoliths, Lithos, 36, 289-303

Hanchar J.M., & Watson, E.B., (2003) Zircon Saturation Thermometry, in John M. Hanchar and Paul W.O. Hoskin, eds., Zircon, Reviews in Mineralogy and Geochemistry, v. 53 p. 183-213, Mineralogical Society of America and Geochemical Society.

Heaman, L.M., Bowins, R., Crocket, J., 1990, The chemical composition of igneous zircon suites : Implications for geochemical tracer studies, Geochimica et Cosmochimica Acta, 54, 1597-1607

Ito, K., Kennedy, G.C., 1971, An experimental study of the basalt-garnet granulite-eclogite transition, in J. G. Heacock, ed., The Structure and Physical Properties of the Earth's Crust. Geophys. Monograph Am. Geophysics Union, Washington.

Jackson, S.E., Pearson, N.J., Griffin, W.L., Belousova, E.A., 2004, The application of laser ablation-inductively coupled plasma-mass spectrometry to in situ U/Pb zircon geochronology, Chem. Geol., 211, pp. 4747e.

Jagoutz, O., 2010, Construction of the granitoid crust of an island arc. Part II: a quantitative petrogenetic model, Contrib. Mineral. Petrol., 160, 359-381

Jagoutz, O., Müntener, O., Schmidt, M.W., Burg, J.P., 2011, The roles of flux- and decompression melting and their respective fractionation lines for continental crust formation: Evidence from the Kohistan arc, EPSL, 303, 25-36

Jagoutz, O., Schmidt, M.W., 2012, The formation and bulk composition of modern juvenile continental crust: The Kohistan arc, Chemical Geology,

Jagoutz, O., 2014, Arc Crustal Differentiation Mechanisms, Earth and Planetary Science Letters, 395, 267-277

Jagoutz, O., & Kelemen, P., 2015, Deep Petrological Processes and Structure of Island Arcs. Annual Review of Earth and Planetary Science, 43, 12.1-12.42

Lee, C.-T, Yin, Q.-Z., Rudnick, R. L., Chesley, J. T., Jacobsen, S. B., 2001, Os isotopic evidence for Mesozoic removal of lithospheric mantle beneath the Sierra Nevada, California. Science, 289, 1912-1916.

Lee, C., Rudnick, R L, Brimhall, G. H., Jr., 2001, Deep lithosphere dynamics beneath the Sierra Nevada during the Mesozoic and Cenozoic as inferred from xenolith petrology, Geochemistry Geophysics Geosystems, 2, 2001GC000152.

Lee, C.T., Cheng, X., Horodyskyj, U., 2005, The development and refinement of continental arcs by primary basaltic magmatism, garnet pyroxenite accumulation, basaltic recharge and delamination: insights from the Sierra Nevada, California, Contrib. Mineral. Petrol., 151, 222-242

Lee, C.T., Thurner, S., Paterson, S., Cao, W., 2015, The rise and fall of continental arcs: Interplays between magmatism, uplift, weathering, and climate, Earth and Planetary Science Letters, 425, 105-119

Manley, C. R., Glazner, A. F., Farmer, G. L., 2004, Timing of volcanism in the Sierra Nevada of California: Evidence for Pliocene delamination of the batholithic root? Geology 28, 811–814

Mattinson, J.M., Graubard, C.M., Parkinson, D.L., McClelland, W.C., 1996, U-Pb Reverse Discordance in Zircons: The Role of Fine-Scale Oscillatory Zoning and Sub-Micron Transport of Pb, in Basu, A., Hart, S eds., Earth Processes: Reading the Isotopic Code, American Geophysical Union

Mattinson, J.M., 2005, Zircon U-Pb chemical abrasion ("CA-TIMS") method: Combined annealing and multi-step partial dissolution analysis for improved precision and accuracy of zircon ages, Chemical geology, 220, 47-66

Mukhopadhyay, B., and Manton, W.I., 1994, Upper mantle fragments from beneath the Sierra Nevada batholith: Partial fusion, fractional crystallization and metasomatism in a subduction-related ancient lithosphere, J. Petrol., 35, 1418–1450

Müntener, O., and Ulmer, P., 2006, Experimentally derived high-pressure cumulates from hydrous arc magmas and consequences for the seismic velocity structure of lower arc crust, Geophys. Res. Lett., 33, L21308

Nasdala, L., Kronz, A., Hanchar, J.M., Tichomirowa, M., Davis, D.W. Hofmeister, W., 2006, Effects of natural radiation damage on back-scattered electron images of single crystals of minerals. American Mineralogist, 91, 1739-1746.

Noyse, H.J., Frey, F.A., Wones, D.R., 1983, A Tale of Two Plutons: Geochemical Evidence Bearing on the Origin and Differentiation of the Red Lake and Eagle Peak Plutons, Central Sierra Nevada, California, Journal of Geology, 91, 487-509

Paton, C., Hellstrom, J., Paul, B., Woodhead, J., Hergt, J., 2011, Iolite: Freeware for the visualization and processing of mass spectrometric data, J. Anal. At. Spectrom., 26, 2508-2518.

Parrish, R.R., and Noble, S.R., 2003, Zircon U-Pb geochronology by isotope dilution – thermal ionization mass spectrometry (ID-TIMS), in John M. Hanchar and Paul W.O. Hoskin, eds., Zircon, Reviews in Mineralogy and Geochemistry, v. 53 p. 183-213, Mineralogical Society of America and Geochemical Society.

Rapp, R. P. & Watson, E. B., 1995, Dehydration melting of metabasalt at 8–32 kbar—implications for continental growth and crust–mantle recycling. Journal of Petrology, 36, 891–931.

Ratajeski, K., Sisson, T.W., Glazner, A.F., 2005, Experimental and geochemical evidence for derivation of the El Capitan Granite, California, by partial melting of hydrous gabbroic lower crust, Contrib. Mineral. Petrol., 149, 713-734

Rubatto, 2002, Zircon trace element geochemistry; partitioning with garnet and the link between U-Pb ages and metamorphism, Chemical Geology, 184, 123-138

Rudnick, R.L., and Taylor, S.R., 1987, The Composition and Petrogenesis of the Lower Crust - a Xenolith Study. Journal of Geophysical Research, 92, ,981-1005.

Rudnick, R.L., Gao, S., 2003, The composition of the continental crust, R.L. Rudnick (Ed.), The Crust, Elsevier, Oxford , pp. 1–64

Rudnick, R.L., Fountain D.M., 1995, Nature and composition of the continental crust: a lower crustal perspective. Rev Geophys, 33, 267–309

Rudnick, R.L., 1995, Making continental crust, Nature, 378, pp. 571–578

Saleeby, J.B., Sams, D.B., Kistler, R.W., 1987, U/Pb zircon, strontium, and oxygen isotopic and geochronological study of the southernmost Sierra Nevada batholith, California, Journal of Geophysical Research 92, 443-453

Saleeby, J.B., 1990, Geochronological and tectonostratigraphic framework of Sierran-Klamath ophiolitic assemblages, in Harwood, D.S., and Miller, M.M., eds., Paleozoic and early Mesozoic paleogeographic relations: Sierra Nevada, Klamath Mountains, and related terranes: Geological Society of America Special Paper 255, p 93-114

Saleeby, J., Ducea, M., Clemens-Knott, D., 2003, Production and loss of high-density batholithic root, southern Sierra Nevada, California, Tectonics, 22(6), 1064

Sisson, T.W., Grove, T.L., Coleman, D.S., 1996, Hornblende gabbro sill complex at Onion Valley, California, and a mixing origin for the Sierra Nevada batholith: Contributions to Mineralogy and Petrology, v. 126, p. 81–108

Sisson, T. W., Ratajeski, K., Hankins, W. B., Glazner, A. F., 2005, Voluminous granitic magmas from common basaltic sources, Contributions to Mineralogy and Petrology 148, 635–661

Stern, T.W., Bateman, P.C., Morgan B.A., Newell, M.F., and Peck, D.L., 1981, Isotopic U-Pb ages of zircons from the granitoids of the Central Sierra Nevada, California: U.S. Geol. Survey Prof. Paper 1185, 17 p.

Tatsumi, Y. & Eggins, S., 1995, Subduction Zone Magmatism. Oxford: Blackwell Scientific.

Taylor, S.R., McLennan, S.M., 1985 The continental crust: its composition and evolution. Blackwell Scientific Publication, Carlton, 312 p

Walker, J.C.G., Hays, P.B., Kasting, J.F., 1981, A negative feedback mechanism for the long-term stabilisation of Earth's surface temperature, J. Geophys. Res., 86, 9776–9782

Whitehouse, M.J., Platt, J.P., 2003, Dating high-grade metamorphism – constraints from rare earth elements in zircon and garnet, Contrib. Mineral. Petrol., 145, 61-74

Wilson, B.M., 1989, Igneous Petrogenesis. A Global Tectonic Approach, Unwin Hyman, 466 p

Winter, J.D., 2001, An introduction to igneous and metamorphic petrology, Prentice Hall, 697p

Wolf, M. B. & Wyllie, P. J., 1994, Dehydration melting of amphibolite at 10 kbar—the effects of temperature and time. Contributions to Mineralogy and Petrology, 115, 369–383.

Zandt, G., Gilbert, H., Owens, T., Ducea, M., Saleeby, J., Jones, C., 2004, Active foundering of a continental arc root beneath the southern Sierra Nevada, California, Nature, 431, 41 – 45

Zellmer, G.F., Annen, C., Charlier, B.L.A., George, R.M.M, Turner, S.P., Hawkesworth, C.J., 2005, Magma Evolution and ascent at volcanic arcs: constraining petrogenetic processes through rates and chronology, Journal of Volcanology and Geothermal Research, 140, 171-191